Experimental Investigations and Modeling of Microwave-Thermal Accelerated-Curing of Concrete

Natt Makul*

Phranakhon Rajabhat University, 9 Changwattana Road, Bangkhen Bangkok, 10220, Thailand

Abstract

The use of microwave energy to acceleratingly cure concretes was presented. First, we measured the dielectric permittivity of concrete during a 24-hour first-hydration period at a operating frequency of 2.45 GHz. Second, we investigated, experimentally and theoretically, the characteristics of concrete as subjected to microwave energy with a multi-mode system, with specific attention to temperature rise, compressive strength, and the use of the maturity function. The results show that dielectric permittivity is relatively high and remains constant during the dormant period. After this period, the hydration reaction resumes and dielectric permittivity decreases rapidly. With the use of microwave heating, early-age strength increases during the first 14 days; however, during the next 14 days, early-age strength decreases slightly, until it reaches its lowest at the 28-day mark. The temperature rise as actually recorded at the center of the specimen during microwave heating in our experiment consistently agreed with figures calculated by a mathematical model.

Keywords: Cementitious materials, Hydration, Microwave energy, Strength

* *Assistant Professor, Building Technology, Faculty of Industrial Technology.*

1. Introduction

By now, microwave (MW) energy has been established as a mature technique with wide-ranging applications in various industrial processes. In particular, 0.915 ± 0.013 GHz and 2.45 ± 0.05 GHz—the two principal microwave frequencies as assigned by the International Microwave Power Institute (IMPI)—are most often used for industrial, scientific, and medical (ISM) purposes. [1] With its rapid and volumetric internal heating, MW has been used widely to heat, dry, and melt various dielectric (non-conducting) materials, such as paper, concrete, wood, rubber, etc., for the related purposes of tempering frozen meat, [2] curing adhesives for lumber, [3] quickly heating of food, [4,5] bonding composite sheets, [6] removing contaminated surfaces, [7,9] treating hyperthermia, [10] and so on.

The use of microwave energy to improve the properties of cement-based materials is a relatively new area of research. However, this is a growing area of interest because microwave heating has many advantages, including high speed for heat generation, high-energy penetration, instantaneous and precise electronic control, and clean process. In addition, conventional curing methods have many limitations. For example, they take a long time to reach the strength required for water curing. [11] In addition, due to the inherent thermal insulation of concrete, they have non-uniform hydration products; [11,12] this causes different tempera-tures to occur in processed concrete under high-stream and temperature-curing conditions.

It is generally accepted that microwaves are electromagnetic waves with frequencies in a range of 300 MHz (10 Hertz [6]) to 300 GHz (10 Hertz [9]) or wavelengths ranging from 39.37 in. (1000 mm) to 0.039 in. (1.0 mm), as shown schematically in the frequency spectrum in Fig. 1.

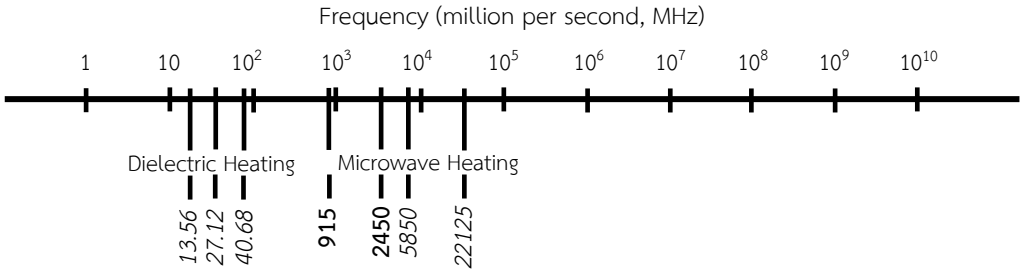

Fig. 1 Electromagnetic spectrum

The term *microwave heating* is equally applicable to microwave systems in both cases; for both, the heating is due to the fact that dielectric material, material with small but finite electrical conductivity, absorbs energy when it is placed in a high-frequency electric field. Consequently, electrical dipole polarization and conduction will be generated within dielectric materials, which are composed of polar molecules with positive and negative poles. These orderly dispersed polar molecules vibrate instantaneously and violently in correspondence to the alternative high-frequency electric field of microwave as shown in Fig 2. It is necessary to overcome the resistance of molecular attraction and motion, because when friction generates heat, the temperature of the material is evaluated simultaneously.

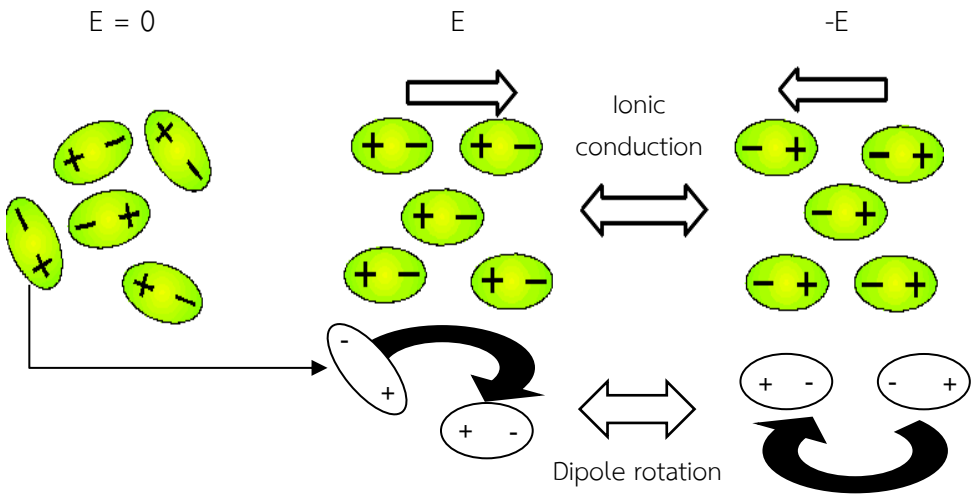

Fig. 2 Mechanisms of microwave heating

The root-mean-square value of the electric field intensity $\vec{E}$ is normally used to evaluate the microwave energy absorbed. Based on Lambert's law, the microwave energy absorbed can be defined in Equation 1. [13]

$$Q = \sigma \left|\vec{E}\right|^2 = 2\pi f \varepsilon_o \varepsilon_r' \left(tan\delta\right) E^2 \qquad (1)$$

where Q is the microwave energy, σ is the effective conductivity, f is the frequency, ε_o is the permittivity of free space (8.8514×10^{-12} Farad/meter), ε_r' is $tan\delta$ is electric field intensity.

When microwave energy travels inwards the dielectric materials, its wave strength fades away exponentially; this occurs because microwave energy is absorbed into dielectric materials and changes to heat. In general, the penetration depth (D_p) denotes the depth at which microwave power density has decreased to 37% or (1/e) of its initial value, as defined in Equation 2.

where D_p is the penetraton depth, ε_r'' is the relative dielectric loss factor, and υ_p is the microwave speed in the dielectric material that can be evaluated by $C/\sqrt{\varepsilon_r'}$.

$$D_p = \frac{1}{\frac{2\pi f}{D_p}\sqrt{\frac{\varepsilon_r'\left(\sqrt{1+\left(\frac{\varepsilon_r''}{\varepsilon_r'}\right)^2}-1\right)}{2}}} = \frac{1}{\frac{2\pi f}{D_p}\sqrt{\frac{\varepsilon_r'\left(\sqrt{1+\left(tan\delta\right)^2}-1\right)}{2}}} \qquad (2)$$

Cementitious materials are dielectric; therefore, their intrinsic properties affect the way they interact with the electric and magnetic fields of microwaves. The dielectric can be characterized by two independent electromagnetic properties, *i.e.,* the complex (electric) permittivity ε^* and the complex (magnetic) permeability μ^*. However, most common cementitious materials are non-magnetic, yielding permeability μ^* that is very close to the permeability of free space ($\mu^* = 4\pi \times 10^{-7}\ Henry/meter$). Thus, this study focuses on the complex ε^*, which comprises real and imaginary parts and can be defined by the relationship expressed in Equation 3.

$$\varepsilon_r^* = \varepsilon_r' - \vec{j}\varepsilon_r'' \quad (3)$$

where ε_r' and ε_r'' are the real part and imaginary parts of the complex permittivity, respectively, and $\vec{j} = \sqrt{-1}$.

The real part of the relative complex permittivity, ε_r', known as the common dielectric constant, is a measure of how much of the energy transferred from an external electric field is stored in a material. The imaginary one, ε_r'', referred to as the relative loss factor, is a measure of how lossy material is to an external electric field. [14] Moreover, an essential ratio of energy lost (relative loss factor) to energy stored (relative dielectric constant) in a material is given as the loss tangent $tan\,\delta$, as shown in Equation 4.

$$tan\,\delta = \varepsilon_r''/\varepsilon_r' \quad (4)$$

2. Research Significance

Previous research studies have clearly indicated that curing by microwave can further increase the early-age strength of cementitious materials. [15–18] However, some aspects have not been taken into account. Thus, this paper investigates the dielectric permittivity of cement-based materials during the initial period of hydration at a frequency of 2.45 GHz. The investigation uses a network analyzer with an open-ended probe technique based on the influences of water-to-cementitious ratios, cement types, pozzolan materials, and aggregates. Secondly, this paper examines the characteristics of hardened cement paste at 24-hour first hydration when the paste has been subjected to a single-mode rectangular wave guide at a frequency of 2.45 GHz.

3. Experimental Investigation

3.1 Materials

Types I and III hydraulic Portland cements were used throughout this test. Their chemical compositions and physical properties are shown in Table 1. The ASTM C 618 [19] classifies the PFA as low calcium (Type F). Silica fume (hereinafter referred to as SF) was also used as a high-pozzolanic material in accordance with the ASTM C 1240. [19]

Table 1 Chemical compositions and physical properties of Type I and Type III Portland cements and pulverized fuel ash (PFA) and silica fume (SF)

Chemical compositions (% by mass)	SiO_2	Al_2O_3	Fe_2O_3	CaO	MgO	K_2O	Na_2O	SO_3	TiO_2	Free CaO
Type I Portland cement	20.84	5.22	3.20	66.28	1.24	0.22	0.10	2.41	0.25	0.99
Type III Portland cement	19.79	5.33	3.02	65.16	1.37	0.32	0.06	3.65	0.23	0.95
Pulverized fuel ash (PFA)	42.10	21.80	11.22	13.56	2.41	1.38	2.90	1.88	0.44	1.44
Silica fume (SF)	97.50	0.40	0.10	0.20	0.10	0.30	0.10	0.20	0.04	0.08

Physical properties	Type I Portland cement	Type III Portland cement	Pulverized fuel ash (PFA)	Silica fume (SF)
Loss on Ignition (%)	0.96	0.82	2.33	0.59
Moisture Content (%)	0.19	0.14	1.50	0.01
Blaine Surface Area (cm^2/g)	3200	3600	2850	25600
Fineness (Particle Size, % Retained)				
- ≥75 μm	0.50	0.14	0.56	0.01
- 75 μm	5.25	2.15	8.25	0.02
- 45 μm	3.60	3.10	4.76	0.01
- ≤36 μm	90.62	94.61	86.43	99.96
Fineness (Retained) on 45 Micron (No. 325)	5.75	9.22	4.90	1.09
Water Requirement (%)	100	103	97	108
Bulk Density (kg / l)	1.03	1.12	0.51	0.43
Specific Gravity	3.15	3.16	2.13	2.24

Tap water with a pH 7.0 and river sand with a fineness modulus of 2.58 and gradation conforming to the ASTM C 33, [19] were mixed in specific proportions. The chemical admixture used superplasticizer that conforms to the ASTM C 494 [19]; that is, the superplasticizer had a recommended dosage rate of 0.02 ounces per 220.46 pound of cementitious materials (500 ml per 100 of a kilogram of cementitious materials). Mineral admixtures included pulverized fuel ash (here-in-after referred to as PFA) from an electricity power plant that used lignite coal as a raw material to produce a combustion-yielding stream for driving the generator.

The proportions of cementitious materials mixed in preparation for specimen testing are shown in Table 2.

Table 2 Mixing proportions of pastes, mortars and concretes

Mix symbol	W/C	A/C	Material constitutes (Air content designed = 1%)					
			Cement	Pulverized fuel ash	Silica fume	Water	Sand	Crushed Lime stone Rock
			lb/ft^3 (kg/m^3)	lb/ft^3 (kg/m^3)	lb/ft^3 (kg/m^3)	lb/ft^3 (kg/m^3)	lb/ft^3 (kg/m^3)	lb/ft^3 (kg/m^3)
CPI0.38	0.38	0	88.46 (1417)	0 (0)	0 (0)	33.59 (538)	0 (0)	0 (0)
CPI0.45	0.45	0	80.53 (1290)	0 (0)	0 (0)	36.15 (579)	0 (0)	0 (0)
CPI0.70	0.70	0	60.74 (973)	0 (0)	0 (0)	42.39 (679)	0 (0)	0 (0)
CPIII0.38	0.45	0	88.59 (1419)	0 (0)	0 (0)	33.65 (539)	0 (0)	0 (0)
CPI0.38SF25	0.38	0	63.55 (1018)	0 (0)	21.04 (337)	31.96 (512)	0 (0)	0 (0)
CPI0.38PFA25	0.38	0	62.30 (998)	20.91 (335)	0 (0)	31.65 (507)	0 (0)	0 (0)
MI0.38	0.38	2.75	35.02 (561)	0 (0)	0 (0)	13.23 (212)	96.51 (1546)	0 (0)
MIII0.38	0.38	2.75	35.02 (561)	0 (0)	0 (0)	13.23 (212)	96.51 (1546)	0 (0)
MI0.38SUPS2.75	0.38	2.75	35.02 (561)	0 (0)	0 (0)	12.92 (207)	96.39 (1544)	0 (0)
MIII0.38SUPS2.75	0.38	2.75	35.02 (561)	0 (0)	0 (0)	12.92 (207)	96.33 (1543)	0 (0)
CI0.38SUP	0.38	4.33	26.53 (425)	0 (0)	0 (0)	9.99 (160)	50.25 (805)	64.30 (1030)
CI0.45SUP	0.45	4.14	26.53 (425)	0 (0)	0 (0)	11.80 (189)	48.13 (771)	61.49 (985)
CI0.70SUP	0.70	3.48	26.53 (425)	0 (0)	0 (0)	18.48 (296)	40.08 (642)	51.82 (830)

Remarks: CP, M and C represent cement paste, mortar and concrete, respectively. I and III represent Types of Portland cement. 0.38, 0.45 and 0.70 represent water-to-cementitious materials (cement/Pulverized fuel ash/ Silica fume). SF and PFA represent silica fume and pulverized fuel ash, respectively. SUP represents superplasticizer, and 2.75, 4.33, 4.14 and 3.48 represent aggregate-to-cementitious ratio.

3.2 Specimen preparation

Three groups of 117 specimens with a cubical shape in size of 2.17 x 2.17 x 4.34 in. [3] (55 x 55 x 110 mm^3) were each tested for dielectric permittivity, temperature increase, and setting time.

For microwave heating, 24 specimens of cement paste were tested. Each one had dimensions of 2.17x2.17x4.34 in. [3] (55x55x100 mm^3). Type I Portland cement and tap water were consistently mixed in accordance with the standard procedures set out in ASTM C 305. [20] The water-to-Type I Portland cement of 0.38 (lb/lb) was kept constant throughout the test. The paste was placed in a mold, which was then wrapped in a plastic sheet prevent water from evaporating out of the paste. At 24 hours after

mixing, the specimens were de-molded; half were then cured by microwave energy, while the others were cured by water at a temperature of 77.0 ± 3.6 °F (25.0 ± 2.0 °C).

3.3 Test procedures

To measure the dielectric permittivity of cementitious materials at a frequency of 2.45 GHz, a network analyzer with an open-ended coaxial probe, [21] as shown in Fig. 3, was used. It consisted of a coaxial cavity; microwave reflectometer; 3.5-mm coaxial cable; 3.5-mm female calibration; and short-, open-, matched-load software. The coaxial cavity characterizes measurement in the range of 1.5–2.6 GHz with precision not more than 2% of the dielectric constant and 5% of the dielectric loss factor. The measured specimen should be assumed; i.e., it should be assumed to have infinite size, non-magnetic material, isotropic and homogeneous properties. In addition, the coaxial cavity must be in contact with the specimen under test (MUT). Under the Nicholson-Ross-Weir [22] conversion process, the dielectric permittivity can be calculated as in Equation 5. After the cementitious material had been mixed and placed in the mold, it was wrapped in Styrofoam that was 0.20 in. (5 mm) thick in order to protect it from heat loss. Both dielectric permittivity and semi-adiabatic temperature using a data logger with thermo-couple (Type K) was simultaneously recorded every 180 and 15 minutes, respectively. However, in order to eliminate the effect of the thermo-couple embedded in microwave radiation, we separately tested three specimens for dielectric permittivity and three for temperature rise. Furthermore, the setting times of pastes, mortars, and cementitious materials were tested by Vicat needle, modified Vicat needle, and penetration resistance in accordance with ASTM C 191, [20] ASTM C 807, [20] and ASTM C 403, [19] respectively.

$$\varepsilon_r^* = \mu_r \frac{(1-\Gamma)^2}{(1+\Gamma)^2}\left(1-\frac{\lambda_0^2}{\lambda_c^2}\right)+\frac{\lambda_0^2}{\lambda_c^2}\cdot\frac{1}{\mu_r} \qquad (5)$$

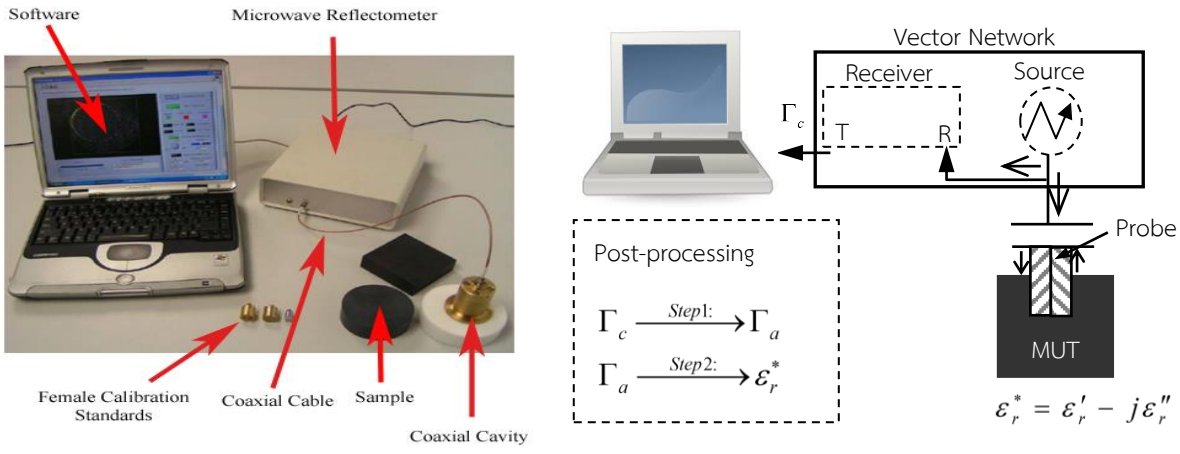

(a) (b)

Fig. 3 A network analyzer (open ended probe technique) (R = reflected, T = transmitted power)

where ε_r^* is the relative permittivity, μ_r is the relative permeability, Γ is the reflection coefficient, and λ_0 and λ_c are the wave length in space and the sample, respectively.

The microwave system used was a mono-chromatic microwave at a frequency of 2.45 GHz, as shown in Fig. 4. [13] Microwave energy was generated by a magnetron and transmitted directly along the propagation direction (+z) of a rectangular wave guide toward a water load situated at the end of the waveguide to ensure that a minimal amount of microwave energy would be reflected back to the sample. A warming water load was circulated through the cooling tower in order to reduce the temperature in the water load system.

A cement paste specimen was arranged perpendicular to the propagation direction. A Type K thermo-couple with a 0.00394 in. (0.1 mm) diameter was inserted at the center of the specimen for the purpose of monitoring the temperature rise. During a 15-minute period of microwave curing, the output of the microwave magnetron was controlled at 1000 watts. The microwave plane wave traveled directly along the wave guide and made contact with the specimen surface; the wave was then reflected and transmitted. By using a wattmeter, incident, reflected and transmitted waves were monitored.

The microwave-cured and water-cured specimens were each tested for compressive strength at the ages of 3, 7, 14, and 28 days, in accordance with ASTM C 39. [19]

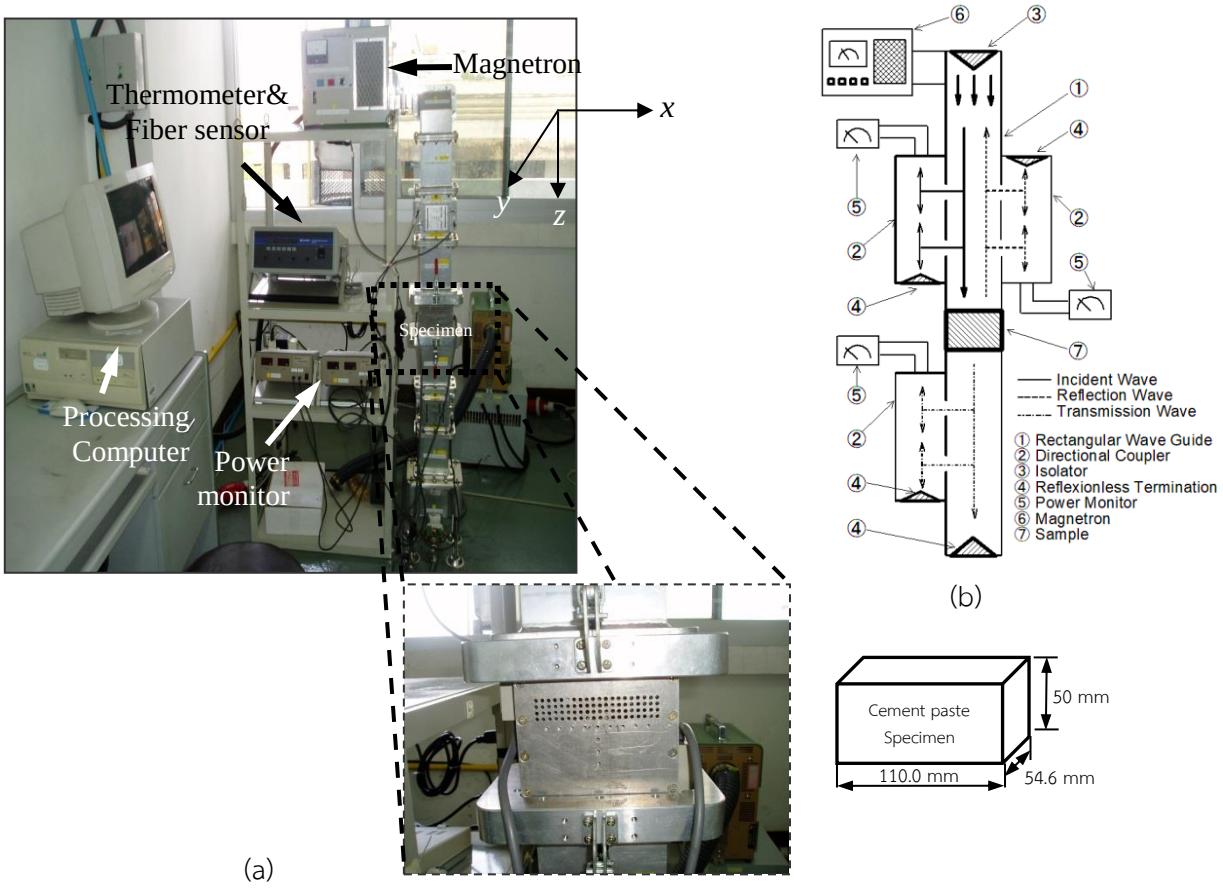

Fig. 4 (a) Experimental set up and (b) Schematic showing flow of microwave radiation

4. Analytical investigation

4.1 A method for predicting the dielectric permittivity of ion-rich water at first contact

4.1.1 Assumptions

(a) Cement-based materials are cement paste (cement with/without mineral admixture, water, air), mortar (cement paste with/without chemical admixture (superplasticizer), fine aggregate (river sand), and cementitious material (mortar and coarse aggregate) crushed limestone rock (maximum size of 10 mm).

(b) Water content and chemical admixture affects the dielectric permittivity of cement-based materials.

(c) After cement particles are brought into contact with water molecules at the end of the induction (dormant) period, the internal structure of the mortar (paste phase plus fine aggregate (river sand)) consists of cement particles, sand particles, and an ion-rich water-based solution that lubricates the solid particles. The solid particles are assumed to be round with difference sizes.

(d) Continuous grain size distribution refers to the fact that the solid grains and air molecules in the cement-based mixture are spherical in shape and have continuous size distribution.

4.1.2 A proposed model

With the help of the complex refract index method, [23] the permittivity of heterogeneous cement-based materials of interest could be based on a given mixture of constituents. If a cement-based material is completely saturated, its permittivity is calculated from the effect of the porosity (ø) of a given mixture and the permittivity of the free water embedded in the mixture; it is also given by:

$$\sqrt{\varepsilon_{mixture}} = \sqrt{\varepsilon' - j\varepsilon''} = (1-\varnothing)\sqrt{\varepsilon_{solidphase}} + (1-S)\varnothing\sqrt{\varepsilon_{air}} + \varnothing S\sqrt{\varepsilon_{water}} \qquad (6)$$

ε_o where ø is the porosity of the mixture (the volume of voids/total volume of mixture), S is the degree of saturation (volume of water/ total volume of voids), $\varepsilon_{solidphase}$ is the relative dielectric permittivity of the mixture solid (dielectric constant), ε_{air} is the relative dielectric permittivity of air (dielectric constant), ε_{water} is the relative dielectric permittivity of water (dielectric constant), and $\varepsilon_{mixture} = \varepsilon' - j\varepsilon''$ is the relative dielectric permittivity of the mixture (dielectric constant).

4.2 A method for calculating temperature rise during microwave curing

4.2.1 Assumptions

(a) In fact, at 23½ ± ½ hours, the hydration reactions of the cement paste progress continuously. This means that heat liberation is produced simultaneously, as shown in Fig. 5. However, in order to simplify the model, heat liberated from hydration reactions is neglected in order to concentrate on eliminating the coupling pheno-mena of heat generation by microwave energy.

(b) From the preliminary study, the final setting time was determined to be 230 minutes for a 0.38-w/c paste; therefore, it may be confirmed that the structure of calcium silicate hydrates—a main structure for setting and hardening the strength in cement paste—was formed completely.

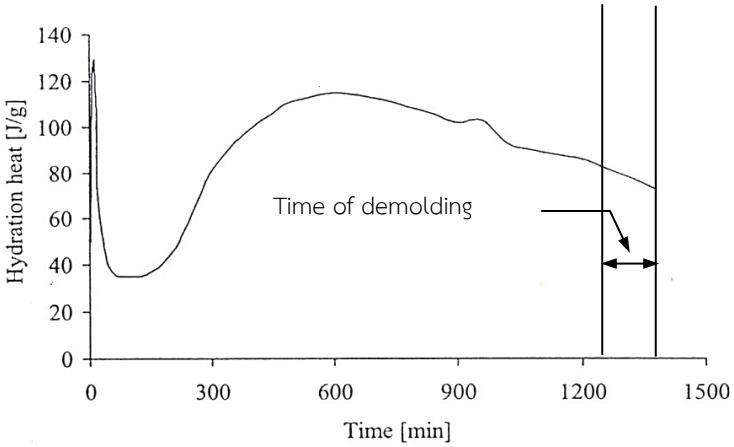

Fig. 5 A typical of heat liberation (J/g) from hydration reactions [28]

4.2.2 Analysis of electromagnetic distribution inside a rectangular wave guide

A plane wave of electromagnetic in TE_{10} mode was taken into account for calculating the electric-magnetic fields. Since a microwave of the TE_{10} mode propagates uniformly in *y*-direction, the electromagnetic field can be considered on the *x–z* plane of a two-dimensional model (Fig. 4). Thus, such correspondent electromagnetic and temperature fields can be contemplated in a two-dimensional model. Fig. 6 illustrates the physical model for the microwave heating of the cement paste using a rectangular wave guide. The proposed model makes the following assumptions: [13]

(a) Cement paste materials (cement plus water) are themselves composed of nonmagnetic materials.

(b) The electrical properties of the rectangular wave guide's walls are perfect conductors that can reflect waves completely.

(c) The absorption of microwave energy by air in the rectangular wave guide is negligible.

(d) The effect of the polyethylene specimen container on the electromagnetic and temperature fields can be neglected.

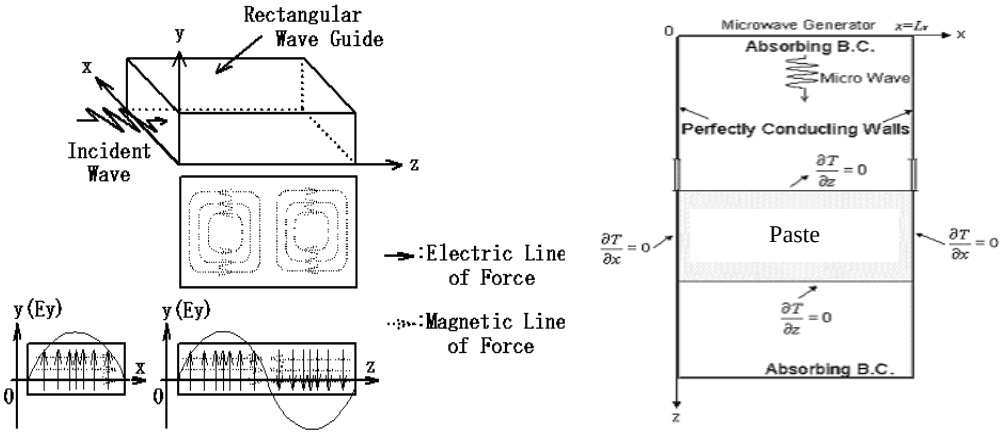

Fig. 6 The electromagnetic field distribution on x-z plane and a physical model

In order to analyze the behavior of electric and magnetic fields in the wave guide, fundamental equations governing the fields, that is, Maxwell's equations, are used. In accord with the above-stated assumptions, the electro-magnetic field can be written in terms of the component notations of electric and magnetic field intensities: [13]

$$\frac{\partial \vec{E}_y}{\partial z}=\mu\frac{\partial \vec{H}_x}{\partial t} \quad (7)$$

$$\frac{\partial \vec{E}_y}{\partial x}=-\mu\frac{\partial \vec{H}_z}{\partial t} \quad (8)$$

$$-\left(\frac{\partial \vec{E}_z}{\partial x}-\frac{\partial \vec{H}_x}{\partial z}\right)=\sigma\vec{E}_y+\varepsilon\frac{\partial \vec{E}_y}{\partial t} \quad (9)$$

where $\vec{E}$ and $\vec{H}$ denote the electric field intensity in (volts per meter (V/m)) and magnetic field intensity (amperes per meter (A/m)), respectively. The subscripts (x, y, and z) represent components of vectors in x, y, and z directions, respectively. Further, the permittivity or dielectric constant, ε (farads per meter, F/m), ε_0 is the permittivity of free space (8.854 × 10 [12] F/m), magnetic permeability, μ and electric conductivity, σ are given by

$$\varepsilon=\varepsilon_0\varepsilon_r,\mu_0,\sigma=2\pi f\varepsilon\left(tan\delta\right) \quad (10)$$

The composite materials of cement paste are non-magnetic. Therefore, the materials effect is negligible, as is true for most dielectric materials used in microwave heating. The cement paste's magnetic permeability (μ) can be approximated by μ_0 in the free space (4π x 10^{-7} H/m).

The boundary conditions associated with the physical model as shown in Fig. 6, are as follows: [13]

(a) Perfectly conducting boundaries. Boundary conditions on the inner wall surface of a rectangular wave guide are given by using Faraday's law and Gauss theorem:

$$\vec{E}_t=0,\vec{H}_n=0 \quad (11)$$

(b) Continuity boundary condition. Boundary conditions along the interface between different materials, for example between air and dielectric material surfaces, are given by using Ampere's law and Gauss theorem:

$$\vec{E}_t=\vec{E}_t^{'},\vec{H}_t=\vec{H}_t^{'},\vec{D}_n=\vec{D}_n^{'},\vec{B}_n=\vec{B}_n^{'} \quad (12)$$

(c) Absorbing boundary condition. At both ends of the rectangular wave guide, the first-order absorbing conditions are applied:

$$\frac{\partial \vec{E}_y}{\partial t}=\pm\upsilon\frac{\partial \vec{E}_y}{\partial z} \quad (13)$$

The symbol ± represents forward or backward waves, and υ is the phase velocity of the microwave.

(d) Oscillation of the electric and magnetic field intensities by magnetron. The incident wave due to the magnetron is given by the following equations:

$$E_y=E_{yim}\,sin\left(\frac{\pi x}{L_x}\right)sin\left(2\pi ft\right) \quad (14)$$

$$H_x=\frac{E_{yin}}{Z_H}sin\left(\frac{\pi X}{L_x}\right)sin\left(2\pi ft\right) \quad (15)$$

Z_H is the wave impedance defined as:

$$Z_H=\frac{\lambda_g Z_I}{\lambda_0}=\frac{\lambda_g}{\lambda_0}\sqrt{\frac{\mu_0}{\varepsilon_0}} \quad (16)$$

The finite difference time domain method was applied to predict the electric and magnetic fields; the leapfrog scheme was implemented using Maxwell's equations. The electric field vector components were offset one half cell in the direction of their corresponding components, while the magnetic field vector components were offset one half cell in each direction orthogonal to their corresponding components. The electric and magnetic fields were both evaluated at every other half-time step. For the TE_{10} mode, the electric field and magnetic field components are expressed with the total field FDTD equations thus:

$$E_y^{\,n}(i,k)=\frac{1-\frac{\sigma(i,k)\Delta t}{2\varepsilon(i,k)}}{1+\frac{\sigma(i,k)\Delta t}{2\varepsilon(i,k)}}E_y^{\,n-1}(i,k)+\frac{1}{1+\frac{\sigma(i,k)\Delta t}{2\varepsilon(i,k)}}\frac{\Delta t}{\varepsilon(i,k)}\left\{\frac{-\left(H_z^{\,n-1/2}(i+1/2,k)-H_z^{\,n-1/2}(i-1/2,k)\right)}{\Delta x}+\frac{\left(H_x^{\,n-1/2}(i,k+1/2)-H_x^{\,n-1/2}(i,k-1/2)\right)}{\Delta z}\right\} \quad (17)$$

$$H_x^{\,n+1/2}(i,k+1/2)=H_x^{\,n-1/2}(i,k+1/2)+\frac{\Delta t}{\mu(i,k+1/2)}\left\{\frac{E_y^{\,n}(i,k+1)-E_y^{\,n}(i,k)}{\Delta z}\right\} \quad (18)$$

$$H_z^{\,n+1/2}(i+1/2,k)=H_z^{\,n-1/2}(i+1/2,k)-\frac{\Delta t}{\mu(i+1/2,k)}\left\{\frac{E_y^{\,n}(i+1,k)-E_y^{\,n}(i,k)}{\Delta x}\right\} \quad (19)$$

The temperature rise of the processed cement paste under soaking with microwave can be obtained by solving the heat-conduction transport equation with microwave power included as a local electromagnetic heat-generation term:

$$\frac{\partial T}{\partial T}=a\left(\frac{\partial^2 T}{\partial x^2}+\frac{\partial^2 T}{\partial z^2}\right)+\frac{Q}{\rho\cdot C_p} \quad (20)$$

where T is the temperature, a is the thermal diffusivity, ρ is the density, and c_p is the heat capacity at constant pressure. The local electromagnetic heat-generation term Q depends on the electric field distribution defined as:

$$Q=2\pi f\varepsilon_0\varepsilon_r\left(tan\delta\right)E_y^2 \quad (21)$$

The initial condition of the multi-layered materials was defined as $T = T_0$ at $t = 0$, the boundary conditions for solving the heat transport equation. [13]

The heat transport equation (Equation 20) was solved by the method of finite differences. The spatial and the temporal terms are approximated using finite difference equations for the electromagnetic field and temperature field. Ratanadecho [13,24] discretized the heat transport equation as solved on this grid system. The choice of spatial and temporal resolution was motivated by considerations of stability and accuracy. To ensure the stability of the time-stepping algorithm, Δt must be chosen to satisfy the courant stability condition:

The calculation conditions that correspond to Equations (20) and (21), are described as follows: [13]

(a) Each wavelength of the microwave in the computational domain with a frequency of 2.45 GHz has more than 10 subdivisions in the numerical calculation. Thus, the computational domain is conservatively set, such that the spatial resolution of each cell is $\Delta x = \Delta z \le \lambda_{mg} \Big/ 10\sqrt{\varepsilon_r} \approx$ 0.0394 in. (1 mm). Thus, the total 110 x 250 cells in the computational domain were used in the numerical calculation.

(b) Because the propagating velocity of a microwave is very fast as compared with the rate of heat transfer, the different time steps of dt = 1 [ps] and 1 [s] are used for the computation of the electromagnetic field and temperature field, respectively. The spatial step size is dx = dz = 0.0394 in. (1 mm):

$$\Delta t \le \frac{\sqrt{(\Delta x)^2 + (\Delta z)^2}}{\upsilon} \qquad (22)$$

The spatial resolution of each cell is defined as:

$$\Delta x, \Delta z \le \frac{\lambda_g}{10\sqrt{\varepsilon_r}} \qquad (23)$$

(c) Number of grid: N = 110 (width) x 250 (length).

(d) Relative errors in the iteration procedure of 10^{-8} were chosen.

5. Experimental Results and Discussion

5.1 Dielectric permittivity of the constituents of cementitious materials

Table 3 shows dielectric permittivity as a function of the temperature of all cement-based constituents. It consists of dielectric constant (ε') and loss factor (ε'') (Portland cement Types I and III, silica fume, pulverized fuel ash, super-plasticizer, river sand, and crushed limestone rock) as a function of temperature change. It can be separated into three groups of materials including the following:

(a) The powder material group comprises Portland cement Types I and III, silica fume, and pulverized fuel ash. This group shows a narrow range of dielectric constant and loss tangent throughout the temperature range of 86–176 °F (30–80 °C). However the loss factor of the materials has a wide variation that is greater that its dielectric constant; this is due to ε' having a high variation, and it is related to the conductivity of a material's polarization and relaxation behaviors.

(b) The water-based materials group consists of water and superplasticizer (polycarboxylic water-based). It has a reasonably wide range of both properties. This is because water is a dielectric material with ε' and $tan\,\delta$ much higher than that of the other components. [1] This effect shows clearly in chemical admixtures that consist mainly of water and polymer. In fact, the manufacturer specified that the solid content of superplasticizer is 40% by weight. Thus, the dielectric properties of admixtures are strongly influenced by water content.

(c) The aggregate materials group, for example, the fine aggregate (river sand) and the coarse aggregate (crushed limestone rock), has dielectric properties that are narrower than those of the powder and water-based material groups. For the dielectric constant under the same compaction condition, fine aggregate materials show a lower value than powder materials because the former is looser in its consistency.

Table 3 Dielectric constant (ε') and loss factor (ε'') of constituents

Constituents	Dielectric constant (ε'); $\varepsilon'(t)=at^3+bt^2+ct+d$			
	$a \pm$ s.d.	$b \pm$ s.d.	$c \pm$ s.d.	$d \pm$ s.d.
Portland cement Type I	-3.671E-07 ± 1.276E-06	3.529E-05 ± 1.869E-04	-2.014E-03 ± 8.294E-03	3.712E+00 ± 4.803E-01
Portland cement Type III	-1.122E-07 ± 1.599E-06	4.021E-05 ± 1.007E-04	-1.476E-03 ± 5.356E-03	6.023E+00 ± 3.911E-01
Pulverized fuel ash	3.333E-07 ± 3.215E-06	-6.667E-05 ± 5.508E-04	4.200E-03 ± 2.859E-02	4.138E+00 ± 3.109E-01
Silica fume	-3.500E-07 ± 7.071E-08	5.500E-05 ± 2.121E-05	-3.350E-03 ± 1.344E-03	2.217E+00 ± 1.790E-01
Superplasticizer (polycarboxylic water-based)	-2.333E-05 ± 8.083E-05	4.767E-03 ± 9.935E-03	-3.260E-01 ± 2.989E-01	2.865E+01 ± 1.933E-01
Fine aggregate (River sand)	-1.000E-08 ± 7.000E-08	-2.333E-06 ± 1.079E-05	2.333E-04 ± 6.429E-04	2.600E+00 ± 1.565E-01
Coarse aggregate (Crushed limestone rock	-8.500E-08 ± 1.626E-07	2.600E-05 ± 4.808E-05	-1.950E-03 ± 3.606E-03	1.224E+00 ± 1.409E-01
Cementitious constituents	Loss factor (ε''); $\varepsilon''(t)=et^3+ft^2+gt+h$			
	$e \pm$ s.d.	$f \pm$ s.d.	$g \pm$ s.d.	$h \pm$ s.d.
Portland cement Type I	3.333E-08 ± 4.989E-08	-7.667E-06 ± 1.115E-05	5.000E-04 ± 7.874E-04	1.565E-01 ± 1.844E-02
Portland cement Type III	7.987E-08 ± 3.043E-08	-3.008E-06 ± 9.453E-06	6.225E-04 ± 2.114E-04	3.922E-01 ± 1.042E-02
Pulverized fuel ash	-1.800E-07 3.111E-07	2.650E-05 4.738E-05	-1.500E-03 2.687E-03	2.763E-01 7.092E-02
Silica fume	-3.667E-07 ± 2.082E-07	6.333E-05 ± 3.512E-05	-3.733E-03 ± 1.850E-03	2.223E-01 ± 2.045E-02
Superplasticizer (polycarboxylic water-based)	-2.000E-05 ± 1.414E-05	3.400E-03 ± 1.273E-03	-1.664E-01 ± 5.155E-02	9.635E+00 ± 1.025E+00
Fine aggregate (river sand)	7.000E-08 ± 1.224E-08	-2.000E-05 ± 2.633E-06	1.000E-03 ± 1.467E-04	2.645E-01 ± 6.209E-2
Coarse aggregate (crushed limestone rock)	7.000E-09 ± 1.453E-09	-2.000E-06 ± 8.2006E-07	1.000E-04 ± 4.798E-05	5.680E-02 ± 4.334E-03

Remark: *s.d.* = Standard Deviation

5.2 Dielectric permittivity of pastes, mortars, and cementitious materials

5.2.1 Effect of water–to–cementitious materials

Fig. 7 shows the evolution of dielectric permittivity and the simultaneous temperature rise in cementitious materials. It can be observed that the dielectric permittivity at the initial stage is relatively high in comparison with the later stage; it also increases with the increasing water content (higher w/c) of the cementitious material. This is due to the fact that immediately after contact has been made between water and cement, they start to react and then Ca^{2+}, OH^{-}, and SO_4^{2-} ions dissolve into the system. In addition, during the dormant period, the dielectric permittivity changes very little because the chemical compositions of the aqueous remain nearly constant. [27]

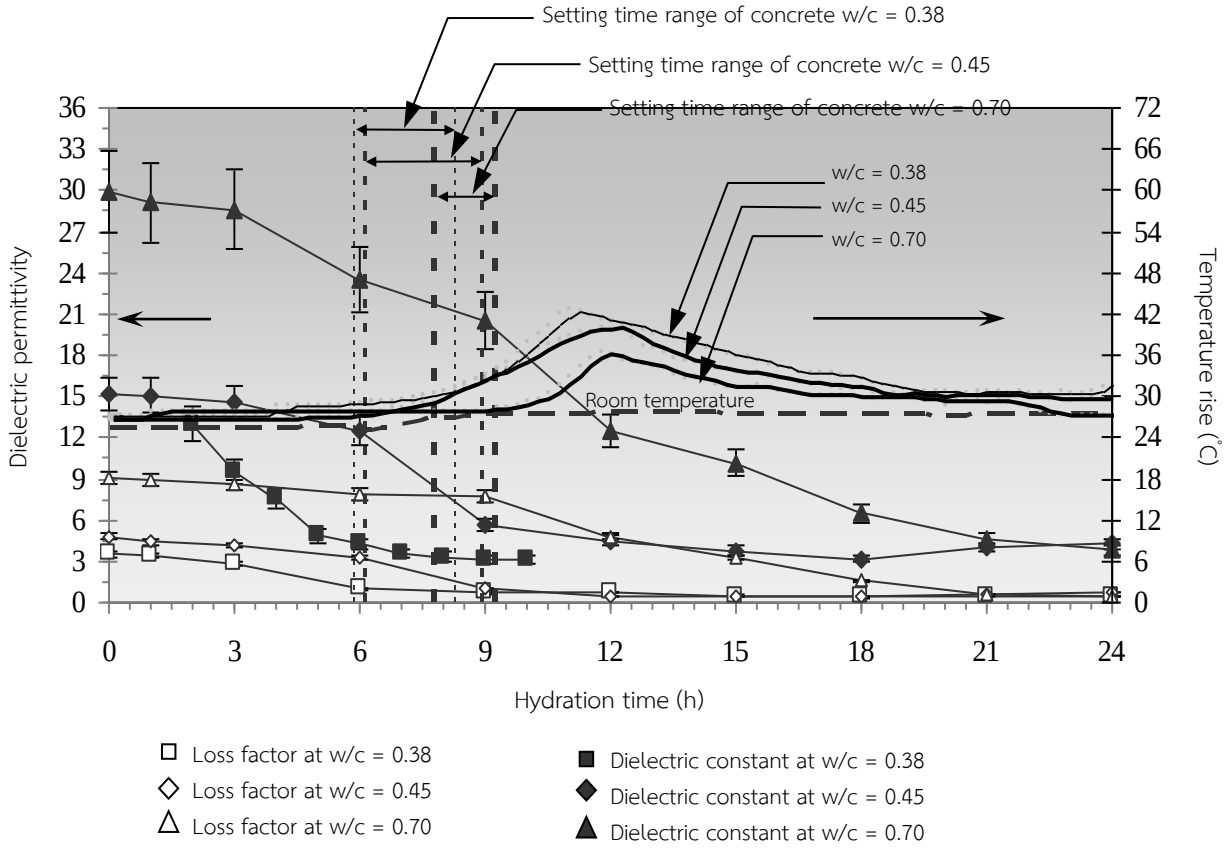

Fig. 7 Dielectric permittivity of concretes with different w/c ratios Temperature in degree Celsius; $T_c = (5/9)*(T_f-32)$; T_c = temperature in degrees Celsius, T_f = temperature in degrees Fahrenheit

5.2.2 Effect of cement types

Fig. 8 shows the changes of permittivity throughout the early stage of the 24-hour hydration reaction period. Permittivity remains at a high level; however, it decreases at the end of the dormant period, approaching a constant value when the internal structure has stabilized. The dielectric permittivity of Type III pastes is higher than that of Type I pastes because Portland cement Type III has finer tri-calcium aluminate (C_3A) grains [26] than Type I. This causes Portland cement Type III to dissolve at a high rate and to maintain an ion-rich system. In addition, the rate at which the dielectric permittivity of Type III paste decreases is higher than that for Type I. In the acceleratory period, the Type III paste reacts faster than the Type I paste does. This coincides with temperature rise and shorter dormant period. For setting time, the dielectric constant is maintained until the final setting time because of the high dissolution rate; however, the dielectric constant drops dramatically with the high hydration rate. At the later stage after formation of the C-S-H structure, the dielectric permittivity tends to remain constant because of the strong constraints imposed by its structure.

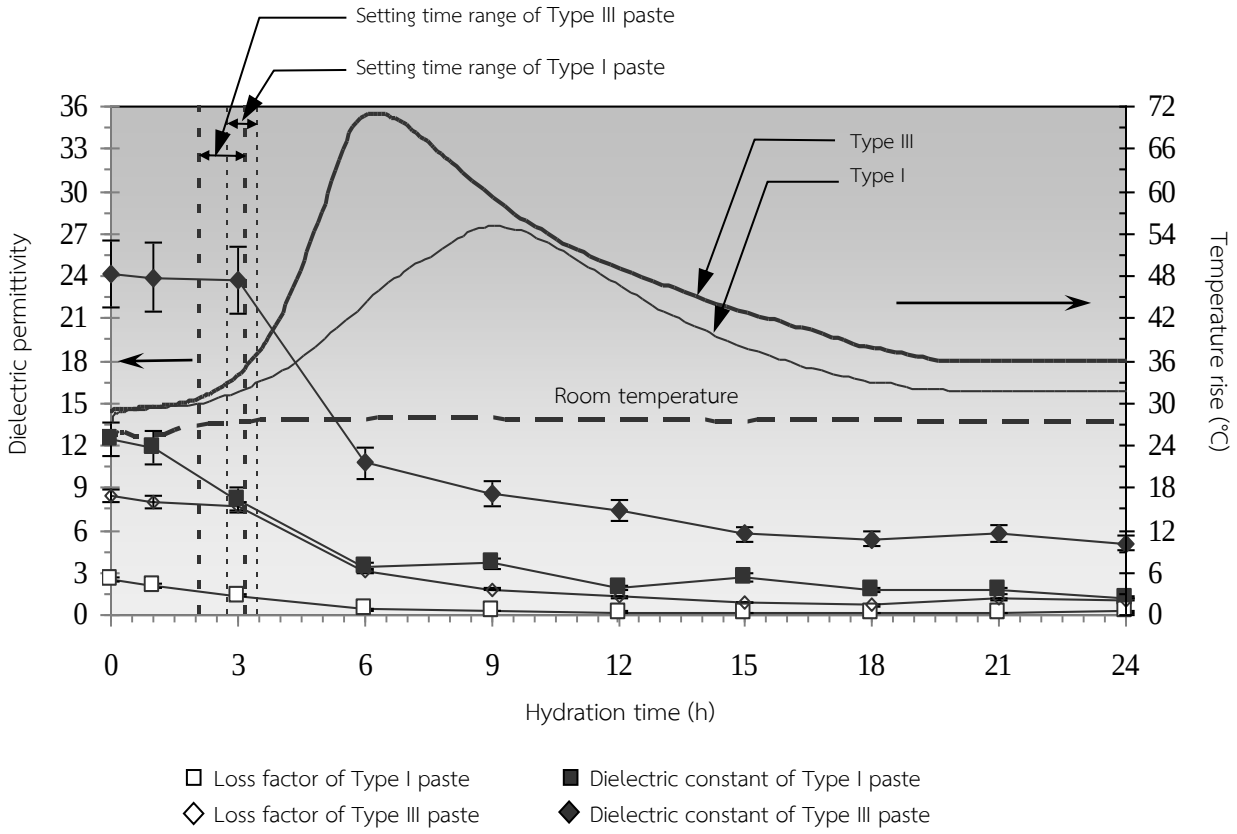

Fig. 8 Dielectric permittivity of pastes with different cement types Temperature in degree Celsius; $T_c = (5/9)*(T_f-32)$; T_c = temperature in degrees Celsius, T_f = temperature in degrees Fahrenheit

5.2.3 Effect of pozzolan materials

Effects of silica fume (SF) and pulverized fuel ash (PFA) on the dielectric permittivity, temperature rise, and setting time of the pastes are shown in Fig. 9. The dielectric constant of the paste containing PFA through the first 24-hour hydration time is higher than that of the plain paste, whereas the paste containing SF is lower. Both reactions involving SF and PFA occur as secondary reactions. This means, however, that the PFA can produce excessive water in the paste while increasing Si^{3+} and Ca^{2+} ions in the system. This results in an increasing dielectric constant of the paste. Unlike the SF paste, the compositions with PFA can dissolve it at a high rate; its fineness induces the bounding of its water molecules and ion-richness at the surface. As a result, the dielectric constant is lower than that of the plain cement paste. For loss factor evolution, the conventional paste and the SF paste show little difference in their comparative loss factors; however between, the difference in the loss factors of the conventional and SF paste when compared with the PFA paste is large. This indicates that the remaining water content, both during introduction and acceleratory periods in the paste, has a strong effect on dielectric loss. On the other hand, the PFA particles can retain free water in the paste system, which may cause the loss factor of the PFA paste to become very high.

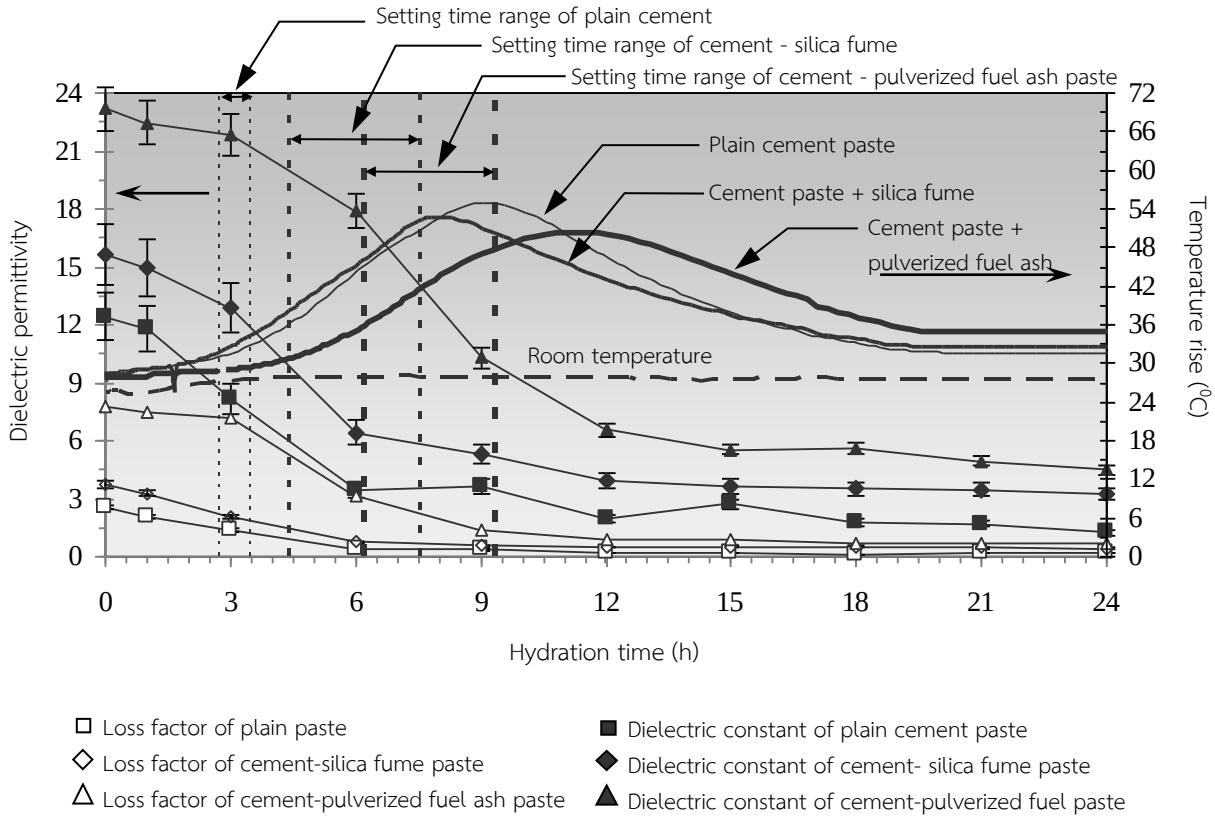

Fig. 9 Dielectric permittivity of pastes with different pozzolan materials Temperature in degree Celsius; $T_c = (5/9)*(T_f-32)$; T_c = temperature in degrees Celsius, T_f = temperature in degrees Fahrenheit

5.2.4 Effect of aggregates

Fig. 10 shows that the relative permittivity curves for the mortar and cementitious material are also similar to the curve of the conventional pastes but lower than that of the pastes. The decrease of cement content and the absorption of water molecules by aggregate surfaces induce a lower concentration of ions in the system. [27] However, eventually, these parameters approach to constant. A comparison in the setting time range shows that the paste's permittivity decrease rate slope is somewhat higher than those of mortars and cementitious materials. This is due to the ion constraints of the hydrated products; specifically that the hydrated products have high ion content in comparison with the aggregate-mixed products.

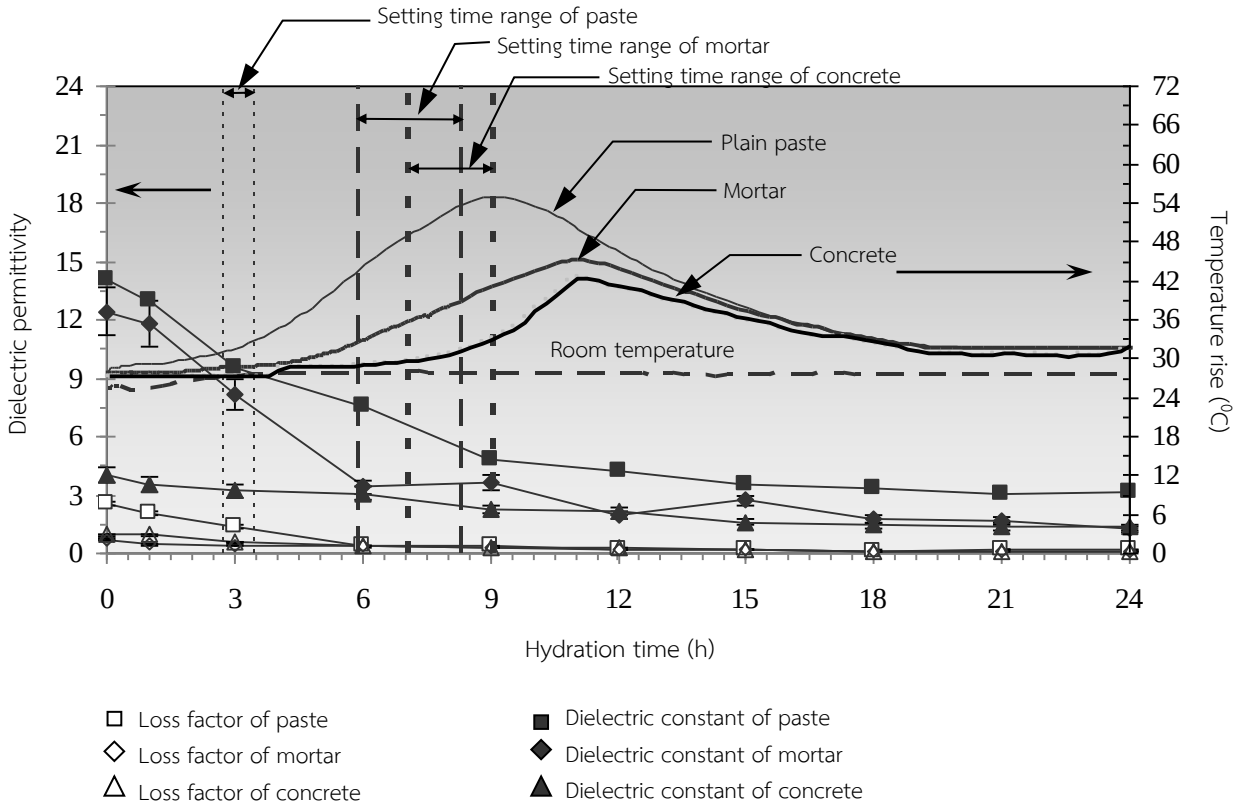

Fig. 10 Dielectric permittivity of paste, mortar and concrete Temperature in degree Celsius; $T_c = (5/9)*(T_f-32)$; T_c = temperature in degrees Celsius, T_f = temperature in degrees Fahrenheit

5.2.5 Temperature rise during microwave curing

The temperature rise at the center of the specimen (Fig.11) shows that temperature continuously increased when the time for microwave curing increased; the temperature increased at a high rate during the early curing period (the first 14 days) and decreased rapidly during the later curing period (the latter 14 days). It is mainly caused by the effect of the amount of water content at the surface of specimen. This means that at early time, high water content caused heat generation to take place within the specimen with high level.

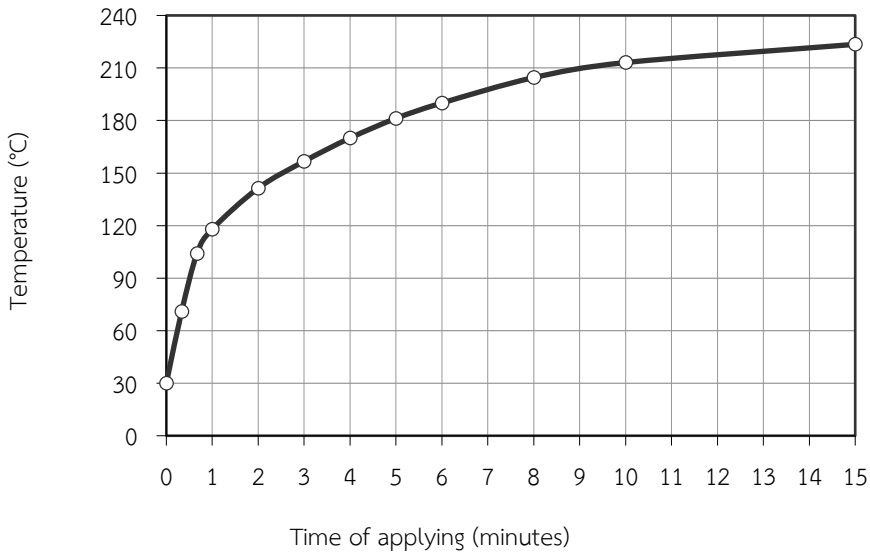

Fig. 11 Temperature rise at the center of the specimen during microwave heating Temperature in degree Celsius; $T_c = (5/9)*(T_f-32)$; T_c = temperature in degrees Celsius, T_f = temperature in degrees Fahrenheit

5.2.6 Compressive strength

Fig. 12 shows the strength development of cement paste after microwave curing as compared to water curing. It can be seen that cement paste cured by microwave has higher strength than the cement paste cured by water. The compressive strengths of both microwave-cured and water-cured cement paste increase quickly from day 1 until day 7. From the figure, the early-age strength of microwave-cured cement paste is clearly superior than the early-age strength of the water cured cement paste. The results indicate that microwave application can significantly increase the degree of hydration during the first few days, after which the microwave-cured specimens and the control specimen attain a similar degree of hydration. After 7 days, the strength appears to become constant; while in the long term the strengths of each of the microwave-cured specimens is slightly lower than for the normal-cured specimens. This is because microwave-cured cement pastes at short time exhibit fewer microcracks; this corresponds to a better micro structure arrangement, and it improves compressive strength. [27] However, after 14 days crossover behavior occurs in regard to the relative strength of the water-cured and microwave-cured cement paste specimens. This takes place due to high early hydration of cement under conditions of overheating. In turn, the overheating may produce a large amount of very fine calcium silicate hydrate (C-S-H) gel, which coats the anhydrates and so hinders diffusion and crystallization of the products of the hydration reactions. These reactions consequently affect the development of long term-strength, specifically. [28]

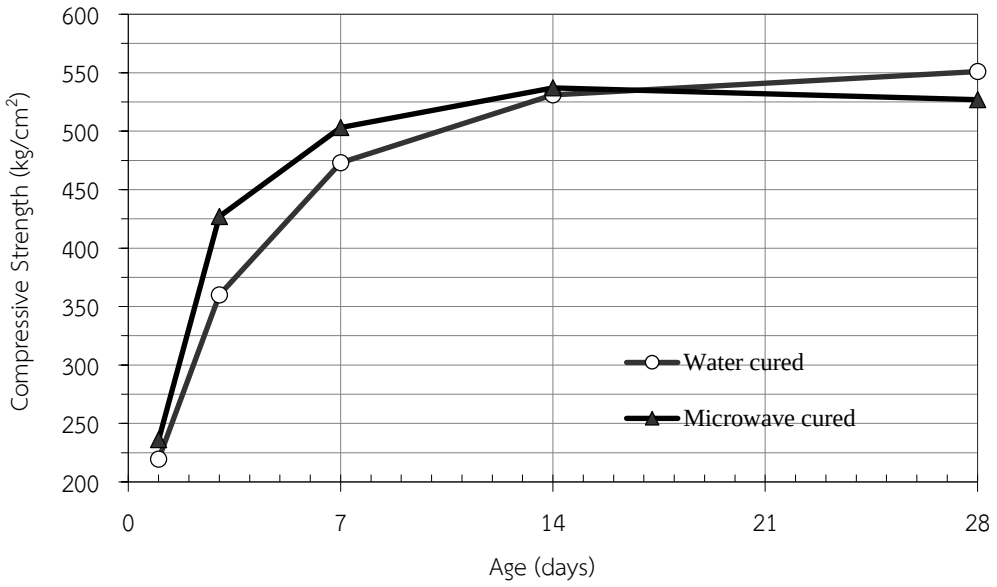

Fig. 12 Comparison of compressive strength development for different curing methods

The maturity index can be approved based on the Arrhenius equation used to describe the effect of temperature on the rate of a chemical reaction. Thus, the equivalent age (t_e) of cement-based materials is set as follows: [28]

$$t_e = \sum_{t=0}^{t=t} e^{\frac{-E}{R}\left(\frac{1}{T(K)}-\frac{1}{T_r(K)}\right)}\Delta t \qquad (24)$$

where t_e is the equivalent age, E is the apparent activation energy (J/mol), R is the universal gas constant (8.314 J/mol. °K), T is the average absolute temperature of cementitious material during time interval Δt (°K), and T_0 is the absolute reference temperature (86 °F (23 °C)).

One simple strength–maturity relationship used the logarithm equation for strength gain under isothermal curing up to an equivalent age at 86 °F (23 °C) for 28 days:

$$S = a + b \cdot log(M) = a + 2.302 \cdot b \cdot ln(M) \qquad (25)$$

where S is the strength at age t, a is the strength for maturity index (M = 1), b is the slope of the line, and M is the maturity index.

According to the Equations (5)–(6) and the ASTM 1074, [19] the relationship of the strength–maturity index can be expressed as in Equation (5). Furthermore, Table 4 reports the value of the referred parameters in order to calculate the strength–maturity relationship:

$$t_e = \sum_{t=0}^{t=t} e^{\frac{-E(J/mol)}{8.314(J/malk)}\left(\frac{1}{(T(°C)+273)(K)}-\frac{1}{T_r(°C)+273(K)}\right)}\Delta t \qquad (26)$$

Table 4 The values use to calculate the relationship

Initial conditions	Value
w/c (by weight)	0.4
Temperature	86 °F (30 °C)
absolute reference temperature	296.15 °K [28]
Apparent activation energy, E (KJ/mol)	0.685 x (T °C) + 18.117 [29,30]

A relationship based on an average of three compressive strengths at each test time against the maturity index is shown in Fig. 13. It can be illustrated that a natural logarithm function with coefficients a = 284.4 and b = 88.2 constituted a best-fit relationship.

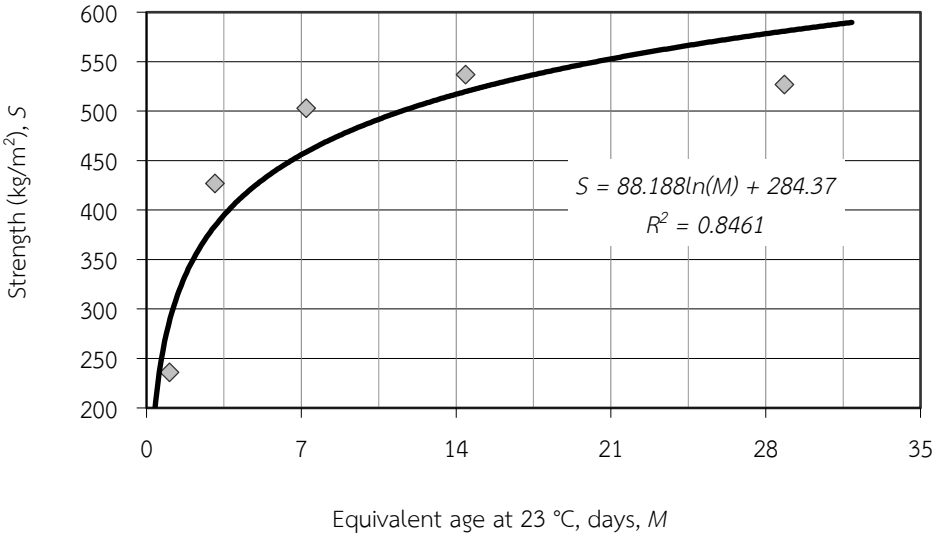

Fig. 13 A strength-maturity relationship of the 0.38-w/c cement paste Temperature in degree Celsius; $T_c = (5/9)*(T_f-32)$; T_c = temperature in degrees Celsius, T_f = temperature in degrees Fahrenheit

5.3 Comparison of predictions and Experimental results

5.3.1 Dielectric permittivity of ion-rich water at first contact

After calculating in accord with the above assumptions and the stated model, the dielectric permittivity of ion-rich water can be summarized as in Table 5. It is found that when cement and water come into contact, the dielectric permittivity of ion-rich water is higher than the permittivity of cement-based materials and mixing water under equal volume fraction. This is because at first contact Ca^{2+} and SO_4^{2-}, etc., dissolve, resulting in an increase in ions in the mix or an increase in the polarization of the water; therefore, dielectric permittivity is very high.

5.3.2 Temperature rise during microwave curing

Electric field dissipation

Fig. 14 shows the electric field distribution within a cement paste specimen during microwave heating. Due to high lossy material in the paste at the age of 1 day after the cement particles and water are mixed together, microwaves' penetrating irradiation occurs at a smaller depth than the depth of specimen. Consequently, a larger part of the microwaves is absorbed by the specimen. It is observed from the figure that the resonance of standing wave configuration inside the small specimen is weak.

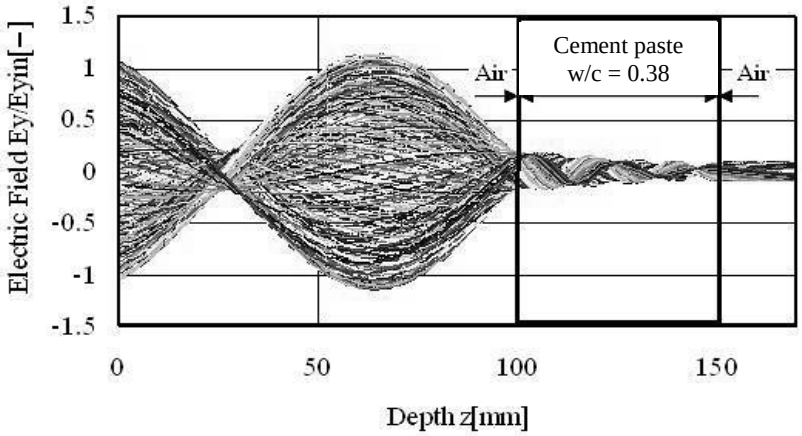

Fig. 14 A typical electric field distribution rectangular wave guide is filled with cement paste sample (t = 60 sec., Power = 1000 W).

5.3.3 Temperature distributions

Fig. 15 exhibits temperature in cement paste between curing by microwave energy. The temperature distributions correspond to the electric field distribution in the processed specimen. This is because attenuation of the electric field when travels through the specimen owing to energy absorption and thereafter the absorbed energy are converted to heat resulted in increase the temperature of the heated cement paste. For example, in addition the temperature distributions are shown for time of application of microwave for 15 minutes bring about the maximum temperature approaches to around 435.20 °F (224 °C). It is observed that the temperature distributions within the paste display a weak wavy behavior due to the penetration depth of microwave drops dramatically and the wavelength is short. Since the reflected wave from the lower surface of the paste is almost negligible, a weak resonance is formed within the paste.

Regarding to tendency of temperature rise within the cement paste, the temperature rise is increased continuously when the heating time of microwave energy increased. The feature trend of temperature increment consists of high rate at the early-age and continuous decrease. It is caused by the effect of penetration depth of absorbed microwave energy and the amount of water content at the surface of the heated specimen. This means that before setting of cement paste, the cement particles settled as gravitational force lead to high porosity or capillary pores with soaked surface near contacting surface to microwave energy.

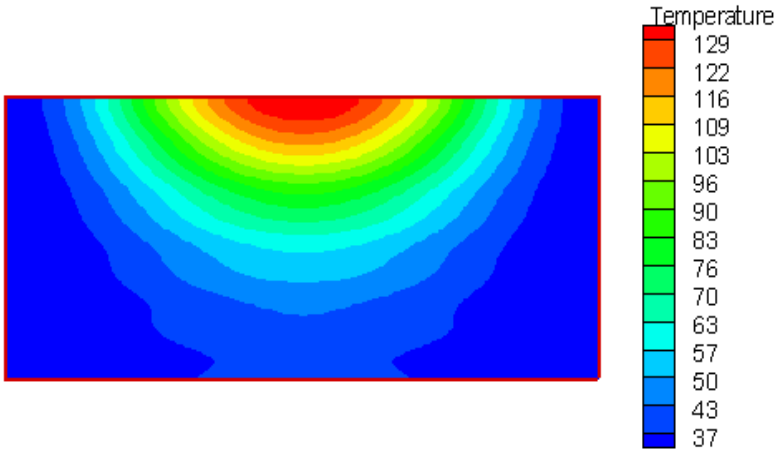

Fig. 15 A typical temperature distribution (°C) at heating times for 60 sec. Temperature in degree Celsius; $T_c = (5/9)*(T_f-32)$; T_c = temperature in degrees Celsius, T_f = temperature in degrees Fahrenheit

6. Further research

Heat and mass transfer mechanisms within the heated cementitious material during curing by microwave energy. A number of works have been proved noticeably that generating and transporting of heat and mass within the heated cementitious material is key factors indicating microwave energy efficiency. This is due to its inherent mechanism of the energy generates heat inside out as volumetrically. However, their assumptions define no chemical reactions occur within the cementitious material in which is considering, but cementitious material is not. The hydration and pozzolanic reactions take place in nature. Therefore, the difficulty of this task, may be defined a point of microwave-cured development is when and how applying microwave energy in a suitable process corresponding to cement reaction.

Numerical tools to predict heat and mass transfer during heating by microwave energy. In almost case of study in microwave energy, numerous models are developed covering in various aspects such as the work of Rattanadecho [13,24] used a three-dimensional Finite Difference Time Domain (FDTD) scheme to determine electromagnetic fields (TE_{10}-mode) and absorbed power by solving the transient Maxwell's equations taking place in microwave with a rectangular wave guide (Fig. 4).

The characteristics of single-mode and multi-mode applicators of microwave system associating with multi-feed hot air system effect on heating mechanisms of cementitious material (Fig. 16). In use of microwave energy to cementitious material, compatibility of microwave heating mechanism and suitable equipments and systems should be considered. In other words, these components should be closely compatible to the cementitious material to be processed. As a matter of fact that heating mechanisms taking place inside multi-mode cavity are somewhat complicated than that of mechanisms occur in the single mode one. However the microwave systems with multi-mode are generally used in industry. The way to solve this problem is to extrapolate the results of single mode exaggerates to predict the phenomena occur in multi-mode cavity as possible.

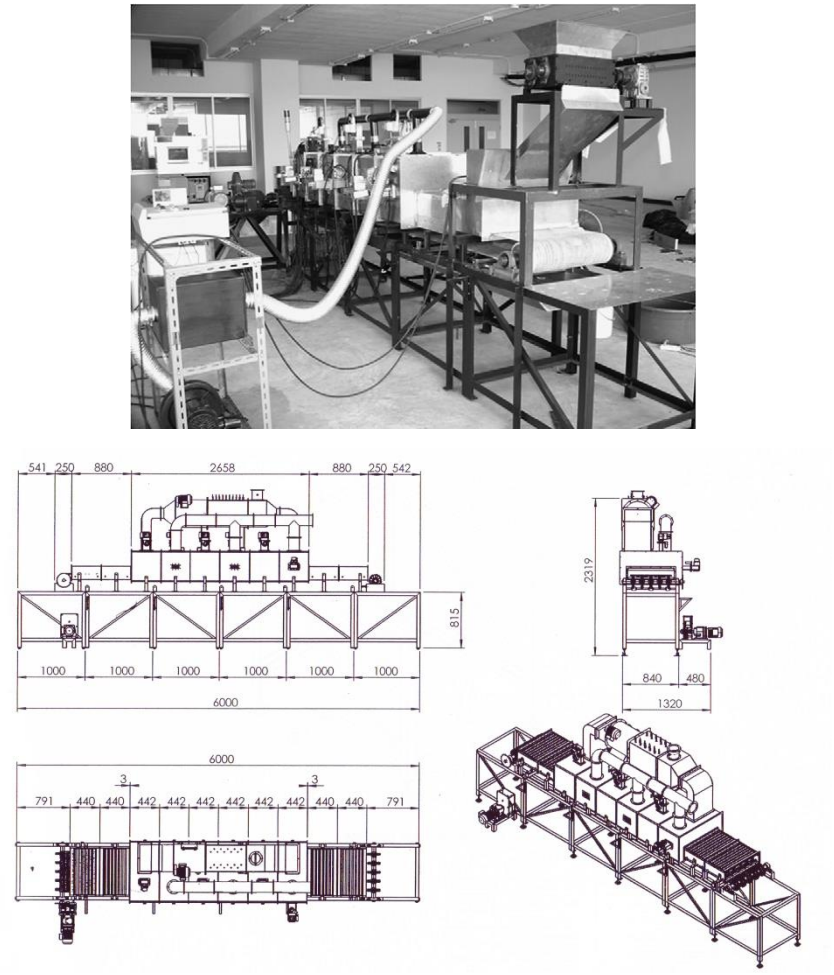

Fig. 16 A combined multi feed microwave-hot air heating with continuous belt system (Multi mode applicator)
Temperature in degree Celsius; $T_c = (5/9)*(T_f-32)$; T_c = temperature in degrees Celsius,
T_f = temperature in degree Fahrenheit

7. Conclusions

The dielectric permittivity of cement-based materials is affected by initial water-to-cement ratio, cement types, pozzolan, and aggregate types. However, though the volumetric fraction of water and superplasticizer in a given mixture is small, it strongly affects the dielectric permittivity of the cement. This is because of the high dielectric permittivity of water and superplasticizer. The change in the dielectric permittivity is relatively high and remains constant during the dormant period; after that it decreases rapidly when the hydration reaction resumes, and it continues to decrease during the acceleratory period.

Under curing by microwave energy using a rectangular wave guide, at the end of the first 14 days (early age) the compressive strength of the hardened cement paste at water-to-Portland cement by mass ratio of 0.38 had increased and then slightly decreased from 14 to 28 days.

Based on the maturity concept, a relationship between the compressive strength of the hardened cement paste and the maturity index is *Compressive Strength = 88.2 × In (Maturity Index) + 284.4.*

8. Acknowledgments

The author appreciates the financial support of the Thailand Research Fund (Contract No. TRG5780255). The author is also grateful for the permission and facilities extended by Professor Dr.Phadungsak Rattanadecho at the Center of Excellence in Electromagnetic Energy Utilization in Engineering (CEEE) at Thammasat University in Thailand.

9. Notation

B	magnetic flux density [Wb/m^2]
D	electric flux density [C/m^2]
E	electric field intensity [V/m]
f	frequency of incident wave [Hz]
H	magnetic field intensity [A/m]
Q	local electromagnetic heat generation [W/m^3]
T	temperature [C]
t	time [s]
$tan\,\delta$	loss tangent [-]
Z_H	wave impedance [Ω]
Z_I	intrinsic impedance [Ω]

10. References

1. Metaxas, A.C., 1991, “Microwave Heating” Journal of Microwave Power and Electromagnetic Energy, pp. 237–247.

2. Peyre, F., et al., 1997, “Influence of the Dielectric Property on Microwave Oven Heating Patterns: Application to Food Materials,” Journal of Micro-wave Power and Electromagnetic Energy, Vol. 32, Issue 1: pp. 3–15.

3. Beall, F.C., 2007, “Industrial Applications and Opportunities for Nondestructive Evaluation of Structural Wood Members,” Maderas: Cienciay Tecnologia, Vol. 9, Issue 2: pp. 127–134.

4. Chen, H., 2008, “Simulation Model for Moving Food Packages in Microwave Heating Processes using Conformal FDTD Method”, Journal of Food Engineering, Vol. 88, Issue 3: pp. 294–305.

5. Orsat, V., 2007, “Microwave-assisted Drying of Biomaterials,” Food and Bioproducts Processing, Vol. 85, Issue 3C: pp. 255–263.

6. Sgriccia, N., Hawley, M.C., 1991, “Thermal, Morphological, and Electrical Characterization of Microwave Processed Natural Fiber Composites,” Composites Science and Technology, Vol. 67, Issue 9: pp. 1986-1991.

7. Li, W., Ebadian, M.A., White, T.L., Grubb, R.G, and Foster, D., 1995, “Heat Transfer within a Concrete Slab with a Finite Microwave Heating Source,” International Journal of Heat and Mass Transfer, Vol. 38, No. 5: pp. 887–897.

8. Lagos, L.E., et al., 1995, “Heat Transfer within a Concrete Slab with a Finite Microwave Heating Source,” International Journal of Heat and Mass Transfer, Vol. 38: pp. 880–897.

9. Bažant Z.P., and Zi G., 2003, “Decontamination of Radionuclides from Concrete by Microwave Heating. I: Theory,” Journal of Engineering Mechanics, Vol. 129: pp. 777–784.

10. Arunachalam, K., 2008, “Characterization of a Digital Microwave Radiometry System for Noninvasive Thermometry using a Temperature–controlled Homogeneous Test Load,”, Physics in Medicine and Biology, Vol. 53: pp. 3883–3901.

11. Leung, K.Y.C., and Pheeraphan, T., 1995, “Microwave Curing of Portland Cement Concrete: Experimental Results and Feasibility for Practical Applications,” Construction and Building Materials, Vol. 9, No. 2, pp. 67–73.

12. Hutchinson, R.G., et al., 1991, “Thermal Acceleration of Portland Cement Mortars with Microwave Energy,” Cement and Concrete Research, Vol. 21: pp. 795–799.

13. Ratanadecho, P., 2002, “Microwave Heating Using a Rectangular Wave Guide,” Doctoral Dissertation, Nakaoka University of Technology.

14. Rhim, H. C., and Buyukozturk, O., 1995, “Electromagnetic Properties of Concrete at Microwave Frequency Range,” ACI Materials Journal, Vol. 95–M25: pp. 262–271.

15. Moukwa, M., et al., 1991, “The Influence of the Hydration Process upon Microwave Properties of Cements,” Cement and Concrete Research, Vol. 21: pp. 863–872.

16. Hutchinson, R.G., et al., 1991, “Thermal Acceleration of Portland Cement Mortars with Microwave Energy,” Cement and Concrete Research, Vol. 21: pp. 795–799.

17. Pheeraphan, T., 1997, “Accelerated Curing of Concrete with Microwave Energy,” Doctor of Philosophy Dissertation, MIT.

18. Dongxu, L., and Xuequan, W., 1994, “A Study on the Application of Vacuum Microwave Composite Dewatering Technique in Concrete Engineering,” Cement and Concrete Research, Vol. 24: pp. 159–164.

19. American Society for Testing and Materials, 2008. “Annual Book of ASTM Standard Vol. 4.02,” Philadelphia, PA, USA.

20. American Society for Testing and Materials, 2008, “Annual Book of ASTM Standard Vol. 4.01,” Philadelphia, PA, USA.

21. HP, Dielectric Probe Kit 85070A. Palo Alto, 1992, CA: Research and Development Unit, Test and Measurements Laboratories, Hewlett Packard Corporation.

22. Venkatesh, M.S., Raghevan, G.S.V., 2005, “An Overview of Dielectric Properties Measuring Techniques.” Canadian Biosystems Engineering, Vol. 47: pp 15–29.

23. Udaya, B.H., Sotoodehnia, A., Maser, K.R., and Kausel, E.A., 1993, “Modeling the Electro-magnetic Properties of Concrete,” ACI Materials Journal.

24. Rattanadecho, P., Suwannapum, N., Chatveera, B., Atong, D., and Makul, N., 2008, “Development of Compressive Strength of Cement Paste under Accelerated Curing by Using a Continuous Microwave Thermal Processor,” Material Science and Engineering A, 472, No. 2: pp. 299–307.

25. Hewlett, P.C., 1998, Lea’s Chemistry of Cement and Cementitious Material, 4th Edition, New York: John Wiley & Sons Inc.

26. Taylor, H.F.W., 1997, Cement Chemistry, 2nd Edition, Great Britain: Thomas Telford Publishing.

27. Cario, N., 1993, “The Maturity Method: Theory and Application,” Cement, Concrete & Aggregates, Vol. 6, No. 2: pp. 61–73.

28. Benameur, H.K., Wirquin, E., and Duthoit, B., 2000, “Determination of Apparent Activation Energy of Concrete by Isothermal Calorimetry,” Cement and Concrete Research, Vol. 30: pp. 301–305.

29. Aloia, L.D., and Chanvillard, G., 2002, “Determining the ‘Apparent’ Activation Energy of Concrete E_a—Numerical Simulations of the Heat of Hydration of Cement,” Cement and Concrete Research, Vol. 32: pp. 1277–1289.